Inorganic Chemistry
Article

Inorg. Chem. **2010**, *49*, 4167–4174 **4167**
DOI: 10.1021/ic902533x

Sensitization of Nanocrystalline TiO_2 Anchored with Pendant Catechol Functionality Using a New Tetracyanato Ruthenium(II) Polypyridyl Complex

Prasenjit Kar,[‡] Sandeep Verma,[†] Anik Sen,[‡] Amitava Das,*[,‡] Bishwajit Ganguly,*[,‡] and Hirendra Nath Ghosh*[,†]

[†]*Radiation and Photo Chemistry Division, Bhabha Atomic Research Center, Mumbai, India, and*
[‡]*Central Salt and Marine Chemicals Research Institute (CSIR), Bhavnagar 364002, Gujarat, India*

Received December 19, 2009

We have synthesized a new photoactive ruthenium(II) complex having a pendant catechol functionality ($K_2[Ru(CN)_4(L)]$ (**1**) (L is 4-[2-(4′-methyl-2,2′-bipyridinyl-4-yl)vinyl]benzene-1,2-diol) for studying the dynamics of the interfacial electron transfer between nanoparticulate TiO_2 and the photoexcited states of this Ru(II) complex using femtosecond transient absorption spectroscopy. Steady-state absorption and emission studies revealed that the complex **1** showed a strong solvatochromic behavior in solvents or solvent mixtures of varying polarity. Our steady-state absorption studies further revealed that **1** is bound to TiO_2 surfaces through the catechol functionality, though **1** has two different types of functionalities (catecholate and cyanato) for binding to TiO_2 surfaces. The longer wavelength absorption band tail for **1**, bound to TiO_2 through the proposed catecholate functionality, could also be explained on the basis of the DFT calculations. Dynamics of the interfacial electron transfer between **1** and TiO_2 nanoparticles was investigated by studying kinetics at various wavelengths in the visible and near-infrared region. Electron injection to the conduction band of the nanoparticulate TiO_2 was confirmed by detection of the conduction band electron in TiO_2 ($[e^-]_{TiO_2}^{CB}$) and cation radical of the adsorbed dye ($\mathbf{1}^{\bullet+}$) in real time as monitored by transient absorption spectroscopy. A single exponential and pulse-width limited (<100 fs) electron injection was observed. Back electron transfer dynamics was determined by monitoring the decay kinetics of $\mathbf{1}^{\bullet+}$ and $[e^-]_{TiO_2}^{CB}$. This is the first report on ultrafast ET dynamics on TiO_2 nanoparticle surface using a solvatochromic sensitizer molecule.

1. Introduction

Dye-sensitized solar cells (DSSC) based on mesoporous nanocrystalline semiconductor surface have attracted significant interest because of their potential for developing low-cost devices.[1−3] More recently, significant efforts in this area of research have been directed toward developing a better insight in understanding the factors that actually control the dynamics of the interfacial electron transfer spectroscopy. These are believed to be crucial for the development of alternative to solid-state photovoltaic devices for solar-to-electrical energy conversion.[1−3] Arguably the most essential process, which has a direct relevance for achieving better efficiency of DSSC, is the efficiency of the electron injection from the photoexcited state of the sensitizer dye to the conduction band of the semiconductor and slow back electron transfer reaction from semiconductor to parent dye cation. In this context, design and synthesis of the sensitizer dye molecule could play an important role, as a sensitizer with a wider absorption band in the longer wavelength of the solar spectrum is better suited for this purpose. However, synthesis of such dye molecules generally involves intricate synthetic methodologies and often is not cost-effective. Recently, use of Ru(II)-polypyridyl-based complexes[4−11] as sensitizer molecules has become an attractive choice for the

*To whom correspondence should be addressed. E-mail: hnghosh@barc.gov.in (H.N.G.); ganguly@csmcri.org (B.G.); amitava@csmcri.org (A.D.). Fax: 00-91-22-25505151 (H.N.G.).

(1) O'Regan, B.; Gratzel, M. *Nature* **1991**, *353*, 737.
(2) Hagfeldt, A.; Gratzel, M. *Chem. Rev.* **1995**, *95*, 49.
(3) (a) Gratzel, M. *Nature* **2001**, *414*, 338. (b) Kuang, D.; Ito, S.; Wenger, B.; Klein, C.; Moser, J.-E.; Humpry-Baker, R. S.; Zakeeruddin, M.; Gratzel, M. *J. Am. Chem. Soc.* **2006**, *128*, 4146. (c) Robertson, N. *Angew. Chem., Int. Ed.* **2006**, *45*, 2338. (d) Klein, C.; Nazeeruddin, M. K.; Liska, P.; censo, D. D.; Hirata, N.; Palomares; Durrant, J. R.; Gratzel, M. *Inorg. Chem.* **2005**, *44*, 178. (e) Anderson, N. A.; Lian, T. *Coord. Chem. Rev.* **2004**, *248*, 1231. (f) Qin, P.; Zhu, H.; Edvinsson, T.; Boschloo, G.; Hagfeldt, A.; Sun, L. *J. Am. Chem. Soc.* **2008**, *130*, 8570.
(4) Kalyansundaram, K.; Gratzel, M. *Coord. Chem. Rev.* **1998**, *77*, 347.
(5) Nazeeruddin, M. K.; Pechy, P.; Renouard, T.; Zakeeruddin, S. M.; Humphry-Baker, R.; Comte, P.; liska, P.; Cevey, L.; Costa, E.; Shklover, V.; Spiccia, L.; Deacon, G. B.; Bignozzi, C. A.; Gratzel, M. *J. Am. Chem. Soc.* **2001**, *123*, 1613.
(6) Nazeeruddin, M. K.; Humphry-Baker, R.; Gratzel, M.; Murrer, B. A. *Chem. Commun.* **1998**, 719.
(7) Wang, P.; Klein, C.; Humphry-Baker, R.; Zakeeruddin, S. M.; Gratzel, M. *J. Am. Chem. Soc.* **2005**, *127*, 808.
(8) Reynal, A.; Forneli, A.; Martinez-Ferrero, E.; Sánchez-Díaz, A.; Vidal-Ferran, A.; O'Regan, B. C.; Palomares, E. *J. Am. Chem. Soc.* **2008**, *130*, 13558.
(9) Kuciauskas, D.; Monat, J.; Villahermosa, E. R.; Gray, H. B.; Lewis, N. S.; McCusker, J. K. *J. Phys. Chem. B* **2002**, *106*, 9347.
(10) Atobello, S.; Argazzi, R.; Caramori, S.; Contado, C.; Da Fre, S.; Rubino, P.; Chone, C.; Larramona, G.; Bignozzi, C. A. *J. Am. Chem. Soc.* **2005**, *127*, 15342.
(11) Tachibana, Y.; Moser, J. E.; Gratzel, M.; Klug, D. R.; Durrant, J. R. *J. Phys. Chem.* **1996**, *100*, 20056.

Published on Web 03/29/2010

chemists and material scientists because of the intense absorption band in the visible region of the spectrum, relatively long-lived ^{3}MLCT excited states, photostability and synthetic tailorability for achieving the desired changes in redox and spectral properties. The key aim is to achieve a total power conversion efficiency over 10% using appropriate and tailored made sensitizer molecules that could harvest a larger portion of the solar spectrum.

Recently, Meyer and co-workers[12] reported dual sensitization of TiO_2 using $Na_2[Fe(bpy)(CN)_4]$ where they could observe electron injection through cyano ligand (metal to particle charge transfer (MPCT) pathway), as well as through 2,2′-bipyridyl (bpy) ligand (MLCT pathway). The presence of the two charge transfer pathways opens up the possibility of using a broader spectral band for efficient sensitization of the semiconductor surfaces and thereby the solar energy conversion process. Earlier reports reveal that the coordination compounds of the general type $[M(CN)_4(bpy)]^{2-}$ (M is Fe^{II} or Ru^{II}) are known to be highly solvatochromic as the coordinated CN^- moiety in these complexes acts as a strong H-bond acceptor functionalities.[13−17] More recently, Argazzi et al.[18] demonstrated solvatochromic solar cells using the solvatochromic sensitizer molecule ($[Ru(CN)_4(dcb)]^{4-}$ (dcb is 4,4′-(dicarboxylato)-2,2′-bipyridine)), anchored to nanocrystalline TiO_2 films. They have demonstrated that solvents of varying polarity can be used to tune the spectral response and efficiencies of regenerative solar cells. Here, the sensitizer dye molecule was proposed to be anchored through carboxylato functionality. Carboxylate functionality has been used widely by various researchers as anchoring functionality for TiO_2-based nanoparticulate surfaces, but has some intrinsic deficiencies.[19,20] The ground state pK_a of the carboxylates is too low (pK_a ∼3.5) to ensure strong binding and slow desorption of the photosensitizers can actually occur in presence of water,[19] which can limit the long-term stability of the cell. While the pK_a value for the catecholate system is considerably higher (pK_a > 9.6), which ensures more efficient binding with TiO_2 nanoparticles even at higher pH. Rice et al. reported a Ru(II)-polypyridyl complex, where catechol functionality is used for anchoring the photoactive Ru(II) complex onto the TiO_2 semiconductor nanoparticles.[20] In some of our earlier reports, we have detailed synthesis of new catecholate-based sensitizer dye molecules and could reveal an efficient interfacial electron injection to the $[CB]_{TiO_2}$.[21−24]

In designing an efficient solvatochoromic dye using such tetracyanato complexes, the relative binding affinity of the anchoring functionality toward TiO_2 is crucial as solvents of varying polarity may influence the binding efficiency, as well as two competitive interfacial charge transfer processes. Further, no reports on the interfacial electron transfer dynamics using solvatochoromic dye molecules for sensitization of nanoparticulate TiO_2 is available in the literature in the ultrafast time domain. Thus, it is crucial to design new solvatochoromic dye molecule having a strongly coupled anchoring functionality, as well as the $Ru(CN)_4$-moiety and study the interfacial electron transfer dynamics onto the nanoparticulate TiO_2 surfaces in the ultrafast time domain. In this present investigation, we have synthesized a new sensitizer dye molecule, $K_2[Ru(CN)_4(L)]$ (**1**) (L is 4-[2-(4′-methyl-2,2′-bipyridinyl-4-yl)vinyl]benzene-1,2-diol), where the dye molecule (**1**) shows solvatochromic behavior in solvent and solvent mixtures of varying polarity. We have reported detailed interfacial electron transfer dynamics involving photoexcited states of the sensitizer molecule and $[CB]_{TIO_2}$ using femtosecond transient absorption spectroscopy. To the best of our knowledge, this is the first report on ultrafast electron transfer dynamics based on tetracyano ruthenium polypyridyl complex (solvatochoromic dye) for sensitization of nanocrystalline TiO_2.

2. Experimental Section

2.1. Materials. Titaniumtetraisopropoxide ($Ti[OCH(CH_3)_2]_4$) (Aldrich, 97%), $K_4[Ru(CN)_6].3H_2O$, 4,4′-dimethyl-2,2′-bipyridine, 3,4-dimethoxy benzaldehyde, n-butyl lithium, disopropyl amine were procured from Sigma-Aldrich and used as received. THF and isopropyl alcohol were dried and distilled prior to use. Nanopure water (Barnsted System, USA) was used for making aqueous solutions and TiO_2 dispersions. All other reagents were of AR grade and procured from SD. Fine Chemicals (India). HPLC grade acetonitrile (E. Mark, Bombay, India) was used for all spectrophotometric titrations. Solvents were degassed thoroughly with IOLAR grade dinitrogen gas before use in the preparation of standard solutions. 4-methyl-4′-(3,4-dihydroxyphenyl)-2,2′-bpy (L) was synthesized following a previously reported procedure.[25]

2.2. Analytical Methods. Microanalyses (C, H, N) were performed using a Perkin-Elmer 4100 elemental analyzer. FTIR spectra were recorded as KBr pellets, using a Perkin-Elmer Spectra GX 2000 spectrometer; ^{1}H NMR spectra were recorded on a Bruker 500 MHz FT NMR (model: Avance II 500) using DMSO-d_6 as the solvent and tetramethylsilane (TMS) as an internal standard; ESI MS measurements were carried out on a Waters QTof-Micro instrument. Electronic spectra were recorded with a Shimadzu UV-3101 PC spectrophotometer, whereasroom-temperature luminescence spectra were recorded with either Fluorolog (Horiba Jobinyvon) or/Perkin-Elmer LS 50B luminescence spectrofluorometer, fitted with a red-sensitive photomultiplier. Electrochemical experiments were performed on a CH-660A electrochemical instrument with a conventional three-electrode cell assembly. A saturated Ag/AgCl reference and a platinum working electrode were used for all measurements.

2.3. Nanoparticle Preparation. Nanometer-size TiO_2 was prepared by controlled hydrolysis of titanium(IV) tetraisopropoxide.[26,27] A solution of 5 mL of $Ti[OCH(CH_3)_2]_4$ dissolved with 95 mL of isopropyl alcohol (Aldrich) was added dropwise (1 mL/min) to 900 mL of nanopure water (2 °C) at pH 1.5 (adjusted with

(12) Yang, M.; Thompson, D. W.; Meyer, G. J. *Inorg. Chem.* **2000**, *39*, 3738.
(13) Toma, H. E.; Takasugi, M. S. *J. Solution Chem.* **1983**, *12*, 547.
(14) Bignozzi, C. A.; Chiroboli, C.; Indelli, M. T.; Scandola, M. A. R.; Varani, G.; Scandola, F. *J. Am. Chem. Soc.* **1986**, *108*, 7872.
(15) Winkler, J. R.; Creutz, C.; Sutin, N. *J. Am. Chem. Soc.* **1987**, *109*, 3470.
(16) Garcia Posse, M. E.; Katz, N. E.; Baraldo, L. M.; Polonuer, D. D.; Colombano, C. G.; Olabe, J. A. *Inorg. Chem.* **1995**, *34*, 1830.
(17) Timpson, C. T.; Bignozzi, C. A.; Sullivan, B. P.; Kober, E. M.; Meyer, T. J. *J. Phys. Chem.* **1996**, *100*, 2915.
(18) Argazzi, R.; Bignozzi, C. A.; Yang, M.; Hasselmann, G. M.; Meyer, G. J. *Nano Lett.* **2002**, *2*, 625.
(19) Nazeeruddin, M. K.; Zakeeruddin, S. M.; Humphry-Baker, R.; Jirousek, M.; Liska, P.; Vlachopoulus, N.; Skhlover, V.; H Fischer, C.; Gratzel, M. *Inorg. Chem.* **1999**, *38*, 6298.
(20) Rice, C. R.; Ward, M. D.; Nazeeruddin, M. K.; Gratzel, M. *New J. Chem.* **2000**, *24*, 651.
(21) Ramakrishna, G.; Jose, D. A.; Kumar, D. K.; Das, A.; Palit, D. K.; Ghosh, H. N. *J. Phys. Chem. B* **2005**, *109*, 15445.
(22) Verma, S.; Kar, P.; Das, A.; Palit, D. K.; Ghosh, H. N. *J. Phys. Chem. C* **2008**, *112*, 2918.
(23) Kar, P.; Verma, S.; Das, A.; Ghosh, H. N. *J. Phys. Chem. C* **2009**, *113*, 7970.
(24) Verma, S.; Kar, P.; Das, A.; Palit, D. K.; Ghosh, H. N. *Chem.—Eur. J.* **2010**, *16*, 611.
(25) Shukla, A. D.; Whittle, B.; Bajaj, H. C.; Das, A.; Ward., M. D. *Inorg. Chim. Acta* **1999**, *285*, 89.
(26) Bahnemann, D.; Henglein, A.; Lilie, J.; Spanhel, L. *J. Phys. Chem.* **1984**, *88*, 709.
(27) Ghosh, H. N. *J. Phys. Chem. B* **1999**, *103*, 10382.

Scheme 1. Synthetic Procedure Followed for Complex **1**

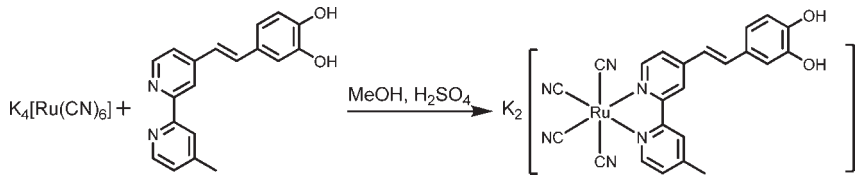

HNO_3). The solution was continuously stirred for 10−12 h until a transparent colloidal solution was formed. This was concentrated at 35−40 °C with a rotary evaporator and then dried with a nitrogen stream to yield a white powder. In the present work all colloidal samples were prepared after dispersing the dry TiO_2 nanoparticles in water (15 g/L).

2.4. Femtosecond Visible Spectrometer. The femtosecond tunable visible spectrometer has been developed based on a multipass amplified femtosecond Ti:sapphire laser system from Avesta, Russia (1 kHz repetition rate at 800 nm, 50 fs, 800 μJ/pulse) and is described in our earlier publications.[28] The 800 nm output pulse from the multipass amplifier is split into two parts to generate pump and probe pulses. In the present investigation, we have used both 800 nm (fundamental) and its frequency-doubled 400 nm as excitation sources. To generate pump pulses at 400 nm one part of 800 nm with 200 μJ/pulse, is frequency doubled in BBO crystals. To generate visible probe pulses, about 3 μJ of the 800 nm beam is focused onto a 1.5 mm thick sapphire window. The intensity of the 800 nm beam is adjusted by iris size and ND filters to obtain a stable white light continuum in the 400 nm to over 1000 nm region. The probe pulses are split into the signal and reference beams and are detected by two matched photodiodes with variable gain. We have kept the spot sizes of the pump beam and probe beam at the crossing point around 500 and 300 μm, respectively. The excitation energy density (at both 800 and 400 nm) was adjusted to ~2500 μJ/cm^2. The noise level of the white light is about ~0.5% with occasional spikes due to oscillator fluctuation. We have noticed that most laser noise is low-frequency noise and can be eliminated by comparing the adjacent probe laser pulses (pump blocked vs unblocked using a mechanical chopper). The typical noise in the measured absorbance change is about $<0.3\%$. The instrument response function (IRF) for 400 nm excitation was obtained by fitting the rise time of the bleach of sodium salt of meso tetrakis (4 sulfonatophenyl) porphyrin (TPPS) at 710 nm and found to be 120 fs.

2.5. Computational Methodology. All calculations were performed with density functional program DMol^3 in Material Studio (version 4.1) of Accelrys Inc.[29] using GGA/PW91/DND,[30] level of theory. The GGA/PW91/DND solvent calculations were performed with COSMO[31] using the gas-phase-optimized geometries. Dielectric constant of water (78.4) was applied.

2.6. Synthesis. $K_2[Ru(CN)_4(L)]$. A mixture of 0.152 g (0.5 mmol) of L and 0.230 g (0.5 mmol) of $K_4[Ru(CN)_6]\cdot 3H_2O$ was suspended in 20 mL of MeOH-H_2O (1:1, v/v). The pH of the resulting dispersion was adjusted between 3 and 4 using dilute sulphuric acid and was set to reflux for 18 h. The color of the solution turned pale yellow. The reaction mixture was cooled to the room temperature and was further neutralized with aqueous solution of K_2CO_3 and solvents of the neutralized reaction mixture were removed under vacuum. The residue was redissolved in water and filtered to remove any unreacted ligand. The filtrate was again evaporated to dryness. The residue was dissolved in methanol, and unreacted $K_4[Ru(CN)_6]$ was then also filtered off as an insoluble residue. The solvent was then removed under reduced pressure and the residue was redissolved in the minimum amount of water (~10 mL). The desired compound was precipitated as yellow solid on addition of acetone (~ 100 mL). This was filtered and washed thoroughly with acetone and then the product was dried in vacuum. Yield: 25%. Negative ion ESI-Ms: m/z 509 (M^+-2K^+). ^{1}H NMR (DMSO, δ ppm): 9.18 (2H, d, J = 5.5 Hz, H^{bpy}); 8.49 (1H, s, H^{bpy}); 8.23−8.12 (4H, m, H^{bpy}, $H^{HC=C-}$, $2H^{phenyl}$); 7.24 (4H, d, J = 5.5 Hz, H^{phenyl}, $H^{HC=C-}$, $2H^{bpy}$); 2.44 (3H, s, H^{-CH_3}). IR 3439(ν_{O-H}), 2093, 2057 ($\nu_{C\equiv N}$). Elemental anal. Found for $C_{23}H_{16}N_6O_2K_2Ru$: C, 41.7; H, 2.5; N, 12.6. Calcd: C, 41.50; H, 2.40; N, 12.63. $E_{1/2}{}^{RuII/III}$: 0.88 V (ΔE ($E_{1/2}{}^A - E_{1/2}{}^B$) = 70 mV) in water and 0.86 V (ΔE ($E_{1/2}{}^A - E_{1/2}{}^B$) = 80 mV) in dimethyl sulphoxide vs Ag/AgCl.

3. Results and Discussion

3.1. Synthesis. The synthetic methodology adopted for the synthesis of complex **1** is outlined in Scheme 1. 2,2′-bipyridyl derivative (L) was synthesized following a reported procedure.[32] The complex was prepared by reaction of L with $K_4[Ru(CN)_6]$ in acidic solution under reflux. The product was isolated by neutralizing the reaction mixture with K_2CO_3. The product was purified by washing thoroughly with water and methanol, respectively, and then reprecipitating the product from aqueous solution with acetone. The identity of the complex was confirmed by the negative ion ES-MS and analytical method. The IR spectra showed the presence of the cyanide stretching vibration.

3.2. Spectroscopic Properties: UV−Vis Absorption and Photoluminescence Measurements. Solvatochromic properties of complex $[Ru(bpy)(CN)_4]^{2-}$ was first reported in 1986 by Bignozzi and co-workers. Since then there are many reports which have described the solvatrochromic effect on $[Ru(CN)_4L]^{2-}$ for solvents with varying polarities. Very recently, Ward et al. have shown that the $Ru_{d\pi} \rightarrow CN^-_{\pi^*}$ based MLCT absorption band in electronic spectra can be appreciably affected with the change in media polarity and the acceptor number of the solvent.[33] It is generally argued that this effect grossly depends on the extent to which the lone pair of electrons at the termini of the cyanide ligands can actually interact with the Lewis acidity of the solvent molecules, which is generally determined on the basis of the respective acceptor numbers of the

(28) Ramakrishna, G.; Singh, A. K.; Palit, D. K.; Ghosh, H. N. *J. Phys. Chem. B*. **2004**, *108*, 1701.

(29) (a) Delley, B. *J. Chem. Phys.* **1990**, *92*, 508. (b) Delley, B. *J. Chem. Phys.* **2000**, *113*, 7756. (c) *Materials Studio DMOL3 Version 4.1*; Accelrys Inc.: San Diego, CA

(30) (a) Perdew., J. P.; Wang, Y. *Phys. Rev. B* **1992**, *45*, 13244. (b) Wu, Z.; Cohen, R. E.; Singh, D. *J. Phys. Rev. B* **2004**, *70*, 104112. (c) Ziesche, P.; Kurth, S.; Perdew, J. P. *Comput, Mater. Sci.* **1998**, *11*, 122. (d) Kohn, W.; Becke, A. D.; Parr, R. G. *J. Phys. Chem.* **1996**, *100*, 12974. (e) Perdew, J. P.; Burke, K.; Ernzerhof, M. *Phys. Rev. Lett.* **1996**, *77*, 3865.

(31) (a) Klamt, A.; Schleyer, P. R.; Allinger, L., Eds., Wiley: New York, 1998, Vol. *2*, 604.(b) Klamt, A. *J. Phys. Chem.* **1995**, *99*, 2224.

(32) Ramakrishna, G.; Jose, D. A.; Kumar, D. K.; Das, A.; Palit, D. K.; Ghosh, H. N. *J. Phys. Chem. B* **2005**, *109*, 15445.

(33) (a) Ward, M. D. *Coord. Chem. Rev.* **2006**, *250*, 3128. (b) Simpson, N. R. M.; Ward, M. D.; Morales, A. F.; Barigelletti, F. *J. Chem. Soc., Dalton Trans.* **2002**, 2449.

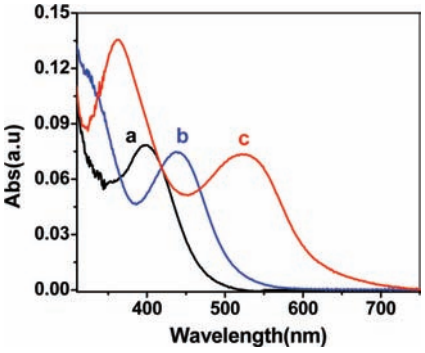

Figure 1. Solvent sensitivity of the MLCT absorption band of complex **1** in (a) water, (b) methanol, and (c) dimethyl sulphoxide.

solvent. Figure 1 shows the optical absorption spectra of **1** in water, methanol, and dimethyl sulphoxide (DMSO). A strong absorption band at 283 nm could be assigned to either the L-based intraligand or the CN^-/L-based interligand $\pi-\pi^*$ transition(s), whereas the broad absorption band between 360 and 500 nm could be predominantly for $Ru_{d\pi} \rightarrow L_{\pi^*}$ based metal to ligand charge transfer (MLCT) transition.[21,23,24] It is very interesting to observe that the MLCT band position changes drastically with the change in solvent from water to methanol to DMSO. It was observed that the MLCT band in water appeared at 397 nm, whereas that in methanol and DMSO appeared at 438 and 524 nm, respectively. Mixed cyano-polypyridine complexes of ruthenium(II) are typical examples in which second sphere donor−acceptor (SSDA) interactions between the cyanides and the solvent produce a pronounced solvatochromic behavior in absorption.[33] The solvatochromic behavior of a solvent depends on the acceptor character of the solvent (as measured by the Gutmann acceptor number)[34] and this provides a relative measure of the Lewis acidity of a particular solvent. It is reported earlier that the photophysical properties of $[Ru(bpy)(CN)_4]^{2-}$ is extremely solvent-sensitive.[14,17] We have recorded steady state absorption and emission spectra of complex **1** in water, dimethyl sulphoxide (DMSO), and in mixtures of these two solvents with varying proportions of DMSO (Supporting Information). As mentioned earlier, absorption maximum for the $Ru_{d\pi} \rightarrow L_{\pi^*}$ was appreciably red-shifted with increasing proportions of DMSO in the solvent mixtures. A similar shift in the steady state emission spectra was also observed—a shift from blue to red region of the spectrum with associated decrease in quantum yield was recorded (see the Supporting Information). The emission intensity of complex **1** was found to be completely quenched in DMSO, which could be explained based on the narrowing of the HOMO−LUMO gap and an effective vibrational deactivation. This phenomena is also supports the energy gap law.

3.3. Electrochemical Measurement. Cyclic voltammogram recorded for complex **1** is shown in Figure 2. $Ru^{II/III}$-based redox process was found to be reversible and $E_{1/2}$ value for this couple was evaluated as 0.88 V (vs Ag/AgCl reference electrode). It was important to evaluate the excited state potential of the sensitizer dye molecule to understand the thermodynamic feasibility of the electron injection process from the excited singlet/triplet

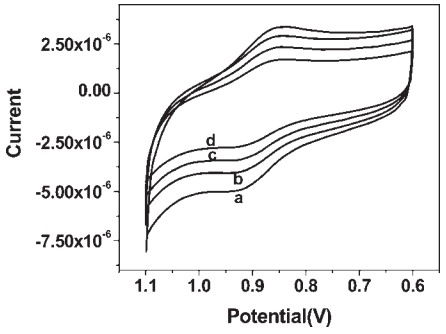

Figure 2. Cyclic voltamogram recorded for complex **1** in water containing $(n\text{-}Bu)_4N.BF_4$ as supporting electrolyte at different scan rates: (a) 300, (b) 200, (c) 100, and (d) 50 mV s^{-1}.

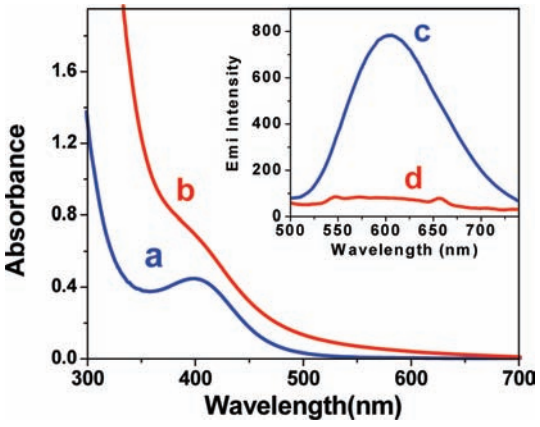

Figure 3. Optical absorption spectra of (a) **1** in water and (b) **1** in TiO_2 nanoparticle (0.5 g/L) dispersion. Inset: emission spectra of (c) **1** in water and (d) **1** in TiO_2 nanoparticle dispersion.

state(s) to the conduction band of the semiconductor particle (TiO_2). E_{0-0} transition energy was 2.03 eV from the intersection of the excitation and emission spectra. Thus the excited state potential, $E(S^+/S^*)$, was −1.15 V] for **1** using the equation $[E(S^+/S^*)] = [E(S^+/S)] - E_{0-0}$ and was found to lie above the conduction band edge of the TiO_2. This supports the thermodynamically feasible electron injection to the conduction band of TiO_2.

3.4. Dye Binding with Nanoparticle. To develop a better understanding on the interfacial electron transfer dynamics it is almost essential to carry out optical absorption studies and compare spectra recorded in absence and presence of TiO_2 nanoparticles. Figure 3 shows the optical absorption spectra of **1** in aqueous solution (Figure 3a) and in dispersion of nanoparticulate TiO_2 in aqueous solution (Figure 3b). Comparison of absorption spectra a and b in Figure 3 revealed that a detectable increase in absorbance with a broadening of MLCT band for the spectra recorded for complex **1** in TiO_2 dispersion. The red shift of the absorption maxima with associated broadening in the visible band up to 650 nm for **1** bound to TiO_2, could be attributed to the strong interaction between the sensitizer molecule **1** and nanoparticles. In our previous reports, we could demonstrate that the interaction between TiO_2 surfaces and dye molecules are very strong for dyes (e.g., $(Ru(bpy)_2(L)^{2+})$,[21] $(Ru(bpy)(SCN)_2(L))$,[23] $Os(bpy)_2(L)^{2+}$,[22,24] alizarin,[28,35] triphenyl

(34) Gutmann, V. *The Donor-Acceptor Approach to Molecular Interactions*; Plenum: New York, 1980.

(35) Kaniyankandy, S.; Verma, S.; Mondal, J. A.; Palit, D. K.; Ghosh, H. N. *J. Phys. Chem. B.* **2009**, *113*, 3593.

methane (TPM) dyes[36] (pyrogallol red and bromo-pyrogallol red) and porphyrin),[37] which are bound to the TiO_2 surfaces through chatecolate functionality. Interestingly, formation of a strong five membered charge transfer complex between chatecolate functionality and TiO_2 is proposed by other researchers too.[38,39] Thus, it can be conclusively emphasized that **1** interacts strongly with TiO_2 nanoparticles with the formation of a five-membered charge transfer complex. However, it is also reported in the literature that TiO_2 nanoparticles and $[Fe^{II}(CN)_6]^{4-}$ ions are known to form charge-transfer complexes at low pH with the formation of a new absorption band at 420 nm.[40−43] The iron complex is believed to bind at a surface Ti^{IV} site of TiO_2 by a monodentate CN^- in $(CN)_5Fe^{II}-CN-Ti^{IV}$(particle) and this was corroborated by IR[43] and resonance Raman[44] studies. The 420 nm absorption band was assigned to the metal-to-particle charge-transfer (MPCT) transition.[40−43] So it is apparent that coordinated CN^- may also compete with catechol functionality in forming charge transfer complex in the present **1**/TiO_2 system. Thus, in the present complex, there are two binding sites for the TiO_2 surfaces, namely the coordinated CN^- functionality or the pendant catechol moiety. At this juncture, it is crucial to clarify the binding nature of the sensitizer **1** to nanoparticle surface. To address this apparent confusion, we carried out steady-state luminescence spectroscopy of **1** in water and in TiO_2 nanoparticle dispersion (Figure 3 inset). Following excitation at the MLCT band, luminescence spectra thus recorded showed a broad band in the 500−700 nm region with an emission maximum at 605 nm (Figure 3c). This emission band could be attributed to the MLCT emission of $Ru_{d\pi} \rightarrow L_{\pi^*}$. Upon addition of aqueous dispersion of TiO_2 nanopatricle to this aqueous solution of sensitizer molecule, this luminescence band was found to be completely quenched (Figure 3d). The complete quenching of emission band could be attributed to electron injection from **1** to TiO_2 nanoparticles. Thus, this result tends to confirm that the electron transfer is occurring from metal center to the semiconductor through catecholate moiety of **L** and not through −CN ligand. Thus it can be assumed that the stronger binding of the catecholate functionality nullifies the possibility of anchoring through coordinated CN^- to TiO_2 nanoparticles in the present study. We have also carried out steady state absorption spectroscopy of **1**/TiO_2 system in water and DMSO solvent mixture (see the Supporting Information). Although the pure dye shows characteristic solvatochromism behavior in solvent mixture with varying amount of DMSO (see the Supporting Information), no such change was observed in the optical absorption for **1**/TiO_2 system.

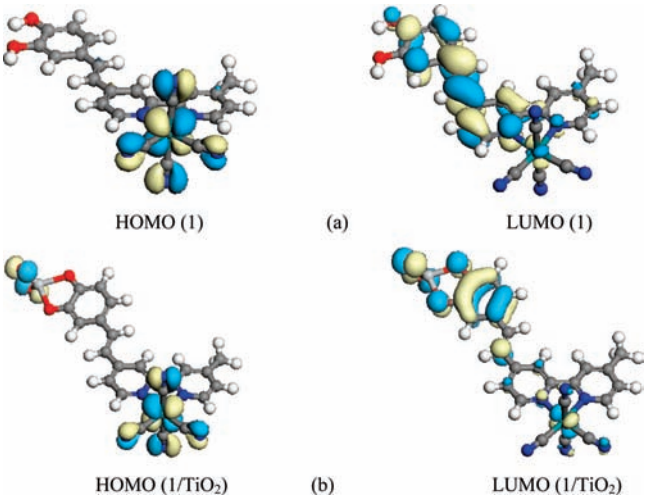

Figure 4. GGA/PW91/DND calculated frontier molecular orbitals for (a) $[Ru(CN)_4L]^{2-}$ in H_2O and (b) **1**/TiO_2 (**1** bound to TiO_2) in H_2O.

3.5. ComputationalStudies. Recently, structural and electronic interactions between the sensitizer molecule and the TiO_2 nanocrystal have been investigated using DFT and TD-DFT calculations.[45] The calculations provide a detailed theoretical understanding of the interactions between the molecular orbitals of the sensitizer with the electronic bands of the substrate that helps to rationalize experimental observations of ultrafast multiexponential photoinduced heterogeneous electron-transfer rates in these systems. The formation of charge transfer complex between catecholate and TiO_2 was examined by Persson et al. through quantum chemical calculations.[45a] The facile interfacial electron injection was inferred due to the formation of a strong charge transfer complex. We have examined the overall blue shift of the observed MLCT band on binding of the Ru-complex to TiO_2 computationally. Figure 4 shows the HOMO−LUMO orbitals obtained from DFT calculations for **1** and the one bound to TiO_2. Employing density functional calculations, using GGA/PW91/DND level, geometries were fully optimized and were taken for the orbital analyses. DFT calculations show that the orbital coefficient of HOMO is largely located on the Ru(II) center and the coordinated CN^- ligands. A larger coefficient was observed on the L for LUMO orbital. Comparison of the frontier molecular orbitals of TiO_2 bound catechol complex (**1**/TiO_2) reveals that the HOMO contains the orbital contributions on Ru(II)-center and coordinated CN^- ligands, similar to the parent $[Ru(CN)_4L]^{2-}$ complex. However, the orbital coefficients are largely concentrated on the catechol bound ring of L for LUMO orbital and not as spread found for parent system. Importantly, the HOMO−LUMO energy difference for **1** in water was predicted to be 2.035 eV, which is in good agreement with the value observed (2.03) from photoelectrochemical

(36) Ramakrishna, G.; Ghosh, H. N.; Singh, A. K.; Palit, D. K.; Mittal, J. P. *J. Phys. Chem. B.* **2001**, *105*, 12786.
(37) Ramakrishna, G.; Verma, S.; Jose, D. A.; Kumar, D. K.; Das, A.; Palit, D. K.; Ghosh, H. N. *J. Phys. Chem. B* **2006**, *110*, 9012.
(38) Moser, J.; Punchihewa, S.; Infelta, P. P.; Gratzel, M. *Langmuir* **1991**, *7*, 3012.
(39) Rajh, T.; Chen, L. X.; Lukas, K.; Liu, T.; Thurnauer, M. C.; Teide, D. M. *J. Phys. Chem. B* **2002**, *106*, 10543.
(40) Nazeeruddin, M. K.; Kay, A.; Rodicio, I.; Humphrybaker, R.; Muller, E.; Liska, P.; Vlachopoulos, N.; Grätzel, M. *J. Am. Chem. Soc.* **1993**, *115*, 6382.
(41) Lu, H.; Prieskorn, J. N.; Hupp, J. T. *J. Am. Chem. Soc.* **1993**, *115*, 4927.
(42) Weng, Y. X.; Wang, Y. Q.; Asbury, J. B.; Ghosh, H. N.; Lian, T. *J. Phys. Chem. B* **2000**, *104*, 93.
(43) Ghosh, H. N.; Asbury, J. B.; Weng, Y.; Lian, T. *J. Phys. Chem. B* **1998**, *102*, 10208.
(44) Blackbourn, R. L.; Johnson, C. S.; Hupp, J. T. *J. Am. Chem. Soc.* **1991**, *113*, 1060.
(45) (a) Persson, P.; Bergström, R.; Lunell, S. *J. Phys. Chem. B* **2000**, *104*, 10348. (b) Persson, P.; Lundqvist, M. J.; Ernstorfer, R.; Goddard, W. A., III; Willig, F. *J. Chem. Theory Comput.* **2006**, *2*, 441. (c) Gundlach, L.; Ernstorfer, R.; Willig, F. *Phys. Rev B* **2006**, *74*, 035324. (d) Persson, P.; Lundqvist, M. J. *J. Phys. Chem. B* **2005**, *109*, 11918. (e) Li, J.; Nilsing, M.; Kondov, I.; Wang, H.; Persson, P.; Lunell, S.; Thoss, M. *J. Phys. Chem. C* **2008**, *112*, 12326.

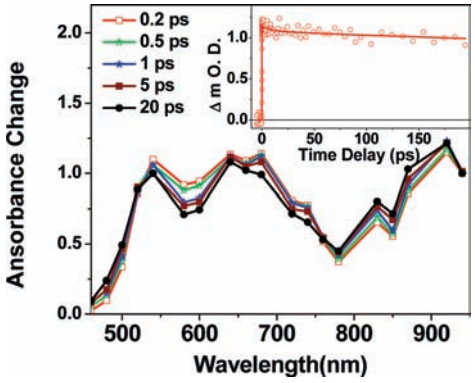

Figure 5. Transient absorption spectra of **1** in water at different delay time following excitation at 500 nm. The transients spectrum shows broad absorption band (490−1000 nm), which have been attributed to the ^{3}MLCT band (triplet−triplet absorption). Insert: Kinetic trace of the excited triplet state (^{3}MLCT) of **1** at 640 nm in water after excitation at 400 nm.

studies. The frontier orbital energy difference was found to be much smaller for TiO_2 bound complex (0.705 eV), which corroborates the shift of absorbance to the longer wavelength.[46]

3.6. Excited State Dynamics of Free Complex 1. To understand photoinduced interfacial electron injection dynamics involving complex **1** and sensitized TiO_2 nanoparticles, it is essential to understand the excited state dynamics of the sensitizer molecule **1** in water. We have carried out transient absorption studies in femtosecond time domain in visible and near-IR region to monitor the excited state dynamics of the sensitizer molecule **1**. Figure 5 shows the transient absorption spectra of **1** in water at different time delays following excitation at 400 nm. The transient spectra show a major absorption band in the wavelength region 500−780 nm with two humps at 540 and 650 nm and another broad band in the near-IR region at 800 nm. The fast growth component was found to be pulse width limited (< 100 fs). The transient absorption bands in the 500 to 780 nm region could be assigned to the excited state absorption (ESA) of **1**. It has been reported in recent literature that intersystem crossing (ISC) process (singlet to triplet) for Ru(II)-polypyridyl complexes is very fast (< 50 fs) and the quantum efficiency for this process is believed to be high (ϕ = 1).[47] Consequently, in the present investigation, we have attributed this ESA to the excited triplet (^{3}MLCT) state absorption, as it is believed that the singlet to triplet conversion might have occurred within the pulse width of the instrument. The kinetic decay trace monitored at 640 nm, following excitation at 400 nm, could be best fitted biexponentially with time constants $\tau_1 = 10$ ps (5.3%) and $\tau_2 = >$ 1 ns (94.3%). It is reported in the literature that the lifetime of the triplet state (^{3}MLCT) of the analogous Ru(II)-polypyridyl complexes are generally > 100 ns.[48] Thus, the longer lifetime of the triplet state is actually reflected in the kinetic traces shown as an insert in Figure 5, which does not decay up to 1 ns.

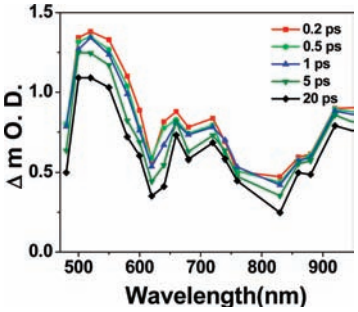

Figure 6. Transient absorption spectra of **1**/TiO_2 nanoparticle in water at different time delay after excitation at 400 nm. Typical concentration for **1** was ~200 μM, whereas that for TiO_2 nanoparticles was ~20 g/L.

3.7. Transient Absorption Measurements of Complex 1/TiO_2. We have already observed in photoluminescence studies, that in presence of TiO_2 nanoparticles, photoluminescence intensity of **1** was drastically reduced and this was attributed to electron injection process involving the photoexcited states of **1** to $[CB]_{TiO_2}$. However, to develop a better understanding about the dynamics of the photoinduced electron transfer processes associated with interfacial electron injection, we carried out time-resolved absorption studies for complex **1/TiO_2** following excitation at 400 nm. Figure 6 shows the transient absorption spectra of **1/TiO_2** at different time delay. The spectrum consists of two broad absorption bands; one is centered at 520 nm with a broad shoulder at 660 nm and the other one ranges from 800 to 1000 nm. The absorption band at higher energy region has been assigned to $\mathbf{1}^{\bullet+}$ (cation radical) formation and the broad absorption band at lower energy region could be attributed to the absorption of injected electron in the conduction band of the TiO_2 ($[e^-]_{TiO_2}^{CB}$). In our earlier investigations, we have observed that all the ruthenium polypyridyl complexes show absorption band due to cation radical in the 500−700 nm region.[21,23,24] The low-energy absorption band in the 800−1000 nm region has been attributed to the conduction band electrons in the nanoparticles.[21−24,28,35,36] Thus, interfacial electron injection time in the present investigation could be determined by monitoring the appearance of the absorption bands for the cation radical of **1** ($\mathbf{1}^{\bullet+}$) at 540 nm and the injected electron at 1000 nm. To determine electron transfer dynamics (both electron injection and back ET), we have monitored the kinetic decay traces at 540 nm which is attributed to cation radical (Figure 7, panel A) and at 1000 nm which is attributed to injected electron (Figure 7, panel B). The injection time has been found to be pulse-width limited (< 100 fs) and single exponential. It is reported by Benko et al.[49] that electron injection is multiphasic in N3-sensitized TiO_2 film, where electron injection takes place both from nonthermalized and thermalized excited states. Slower electron injection from thermalized triplet states has been confirmed by the decay of triplet states with a concomitant growth of cation radicals.[49] However, in the present investigation, we did not observe any such concomitant growth for the cation radical or injected electron. We have

(46) (a) The unreasonably small HOMO−LUMO energy difference for the TiO_2 bound complex obtained by DFT calculation may be due to significant underestimation of the energy gap by the DFT methods. (b) Dufek, P.; Blaha, P.; Schwarz, K. *Phys. Rev. B* **1994**, *50*, 7279. (c) Heyd, J.; Scuseria, G. E. *J. Chem. Phys.* **2004**, *121*, 1187. (d) Zhang, D; Sun, H.; Liu, J.; Liu, C. *J. Phys. Chem. C* **2009**, *113*, 21.

(47) Bhasikuttan, A. C.; Suzuki, M.; Nakashima, S.; Okada, T. *J. Am. Chem. Soc.* **2002**, *104*, 8398.

(48) Vlček, A., Jr. *Coord. Chem. Rev.* **2000**, *200*, 933.

(49) Benko, G.; Kallioinen, J.; Korppi-Tommola, J. E. I.; Yartsev, A. P.; Sundstrom, V. *J. Am. Chem. Soc.* **2002**, *104*, 489.

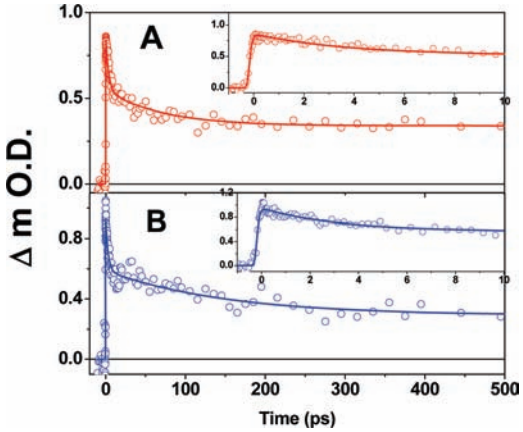

Figure 7. Transient decay kinetics of **1**/TiO_2 (a) in panel A with λ_{mon} = 540 nmm (b) in panel B λ_{mon} = 1000 nm. Insets: decay kinetics in shorter time scale.

monitored transition absorption measurements in the wavelength region from 500 to 1000 nm: Transient signal at all different wavelengths was monitored and found to be single exponential. A pulse-width limited growth and multiexponential decay was observed. Growth and decay dynamics were found to be similar at all wavelengths. In our earlier investigations,[21−24] we did confirm that for related Ru(II)−polypyridyl complex/TiO_2 nanoparticle systems, the spectra recorded are primarily due to the charge-separated species (cation radical and injected electron) and contribution due to excited states is very negligible. In all studies, it was indicated that electron injection took place predominantly from nonthermalized singlet state (^{1}MLCT), and/or nonthermalized triplet state (^{3}MLCT) or a combination of both, which is a unique observation in ET dynamics in Ru(II)-polypyridyl sensitized TiO_2 systems studied so far. Strong coupling in dye-nanoparticle system facilitates ultrafast single exponential electron injection, which competes with thermalization process of the excited states. If at all there is electron injection from the thermalized excited states, we could have seen the growth of the cation radical in early time scale (< 10 ps). However, we did not observe any such growth in transient absorption spectra.

We have also monitored charge recombination dynamics, which is a very important parameter in interfacial ET where the injected electron ($[e^-]_{TiO_2}^{CB}$) recombines with the radical cation center. Recombination dynamics (BET) can be evaluated by monitoring the decay kinetics of either the electron in the conduction band at 1000 nm or the cation radical at 540 nm. We have monitored the kinetic decay trace of the cation radical ($\mathbf{1}^{\bullet+}$) at 540 nm and this could be fitted multiexponentially with time constants τ_1 = 3.5 ps (37.5%), τ_2 = 70 ps (23.9%), and τ_3 > 1 ns (38.6%). The kinetics decay traces at 1000 nm, which has been attributed to the conduction band electron ($[e^-]_{TiO_2}^{CB}$) could be fitted multiexponentially with time constants τ_1 = 3 ps (39.8%), τ_2 = 150 ps (30.6%), τ_3 > 1 ns (29.6%), and these time constants matched closely with those obtained by monitoring the decay traces at 540 nm.

We have also carried out ET dynamics in **1**/TiO_2 system in different solvent mixtures of water and DMSO to check the effect of solvatochromism on interfacial ET dynamics. In the present studies, the sensitizer molecule (**1**) has shown strong solvatochromic effect in solvent mixture of varying proportions of water and DMSO (see the Supporting Information). Ultrafast transient absorption studies of **1**/TiO_2 system in different solvent mixture (ratio of water and DMSO) clearly show that neither the transient spectrum nor the kinetic traces at different wavelengths changes with solvent composition. The effect of solvent on electron injection dynamics has been observed by Lian and coworkes[50] in $Re(LA)(CO)_3Cl$ [LA = dcbpy = 4,4′-dicarboxy-2,2′-bipyridine] sensitized TiO_2 nanocrystalline thin films as studied by transient IR absorption spectroscopy. The Re dye molecules were coupled with TiO_2 film with carboxylate moiety which has been found to more sensitive with solvent and water composition. However, in the present investigation, the Ru dye is coupled with catecholate moiety, where we did not observe any solvent dependency on ET dynamics. In other words dynamics of the interfacial electron transfer in **1**/TiO_2 system does not change with solvent composition. This presumably reflects the strong coupling of complex **1** with TiO_2 nanoparticulates through catecholate functionality, which remain unaffected with change in solvent polarity.

4. Conclusion

We have synthesized a new ruthenium(II)−polypyridyl complex ($[Ru(CN)_4L]^{2-}$, **1**), having a pendant catechol functionality for binding to the nanoparticulate TiO_2 surfaces. Steady-state optical absorption and emission spectra recorded for complex **1** in different solvent and solvent mixtures revealed the solvatochromic behavior of the dye molecule. Although complex **1** possesses two different binding functionalities (coordinated CN^- and the pendant catecholate group), steady-state absorption studies suggest binding to the TiO_2 surfaces through the pendant catecholate moiety of the complex (**1**). Broader absorption band at longer wavelength for the **1**/TiO_2 system as compared to **1** is due to the formation of a strong charge transfer complex. This observation was further corroborated by DFT studies. We have investigated interfacial electron transfer dynamics between the photoexcited states of **1** and the conduction band of TiO_2 nanoparticles using transient absorption spectroscopy. On excitation with 400 nm laser pulse, transient absorption for the dye cation ($\mathbf{1}^{\bullet+}$) and broad absorption band for the conduction band electron are observed. Electron injection was found to be single exponential and pulse width limited (< 100 fs) indicating electron injection from nonthermalized singlet state (^{1}MLCT), and/or triplet state (^{3}MLCT) or a combination of both. Back ET dynamics was studied by monitoring the decay kinetics of cation radical ($\mathbf{1}^{\bullet+}$), and injected electron in the conduction band of TiO_2. Back ET reaction multiexponentially with time constants τ_1 = 3.5 ps (37.5%), τ_2 = 70 ps (23.9%), τ_3 > 1 ns (38.6%). Although complex **1** is a solvatochromic dye, we still did not observe any effect of solvatochromism on interfacial electron transfer dynamics, as the dye couples strongly through catecholate, which diminishs the effect of solvatochromism.

(50) She, C.; Guo, J.; Lian, T. *J. Phys. Chem. B* **2007**, *111*, 6903.

Acknowledgment. BRNS (DAE, India), DST (India), and CSIR (India) have supported this work. P.K. acknowledges CSIR for a Senior Research Fellowship. We thank Dr. P. K. Ghosh (CSMCRI), Dr. S. K. Sarkar (BARC), and Dr. T. Mukherjee (BARC) for their interest in this work.

Supporting Information Available: Absorption and emission spectra of **1** in various water−DMSO mixtures ranging from pure water to pure DMSO solvent combination (Figure 1); optical absorption spectra of complex 1 on TiO_2 nanoparticle surface in water:DMSO solvent mixtures (Figure 2) (PDF). This material is available free of charge via the Internet at http://pubs.acs.org.